

# No surviving evolved companions to the progenitor of supernova SN 1006

Jonay I. González Hernández<sup>1,2</sup>, Pilar Ruiz-Lapuente<sup>3,4</sup>, Hugo M. Tabernero<sup>5</sup>, David Montes<sup>5</sup>, Ramon Canal<sup>4</sup>, Javier Méndez<sup>4,6</sup>, Luigi R. Bedin<sup>7</sup>

<sup>1</sup> Instituto de Astrofísica de Canarias, E-38205 La Laguna, Tenerife, Spain

<sup>2</sup> Departamento de Astrofísica, Universidad de La Laguna, E-38206 La Laguna, Tenerife, Spain

<sup>3</sup> Instituto de Física Fundamental, CSIC, E-28006 Madrid, Spain

<sup>4</sup> Department of Astronomy, Institut de Ciències del Cosmos, Universitat de Barcelona (UB-IEEC), Martí i Franquès 1, E-08028 Barcelona, Spain

<sup>5</sup> Departamento de Astrofísica y Ciencias de la Atmósfera, Facultad de Ciencias Físicas, Universidad Complutense de Madrid, E-28040 Madrid, Spain

<sup>6</sup> Isaac Newton Group of Telescopes, P.O. Box 321; E-38700 Santa Cruz de La Palma, Spain.

<sup>7</sup> INAF-Osservatorio Astronomico di Padova, Vicolo dell'Osservatorio 5, I-35122 Padova, Italy

Type Ia supernovae are thought to occur as a white dwarf made of carbon and oxygen accretes sufficient mass to trigger a thermonuclear explosion<sup>1</sup>. The accretion could occur slowly from an unevolved (main-sequence) or evolved (subgiant or giant) star<sup>2,3</sup>, that being dubbed the single-degenerate channel, or rapidly as it breaks up a smaller orbiting white dwarf (the double-degenerate channel)<sup>3,4</sup>. Obviously, a companion will survive the explosion only in the single-degenerate channel<sup>5</sup>. Both channels might contribute to the production of type Ia supernovae<sup>6,7</sup> but their relative proportions still remain a fundamental puzzle in astronomy. Previous searches for remnant companions have revealed one possible case for SN 1572<sup>8,9</sup>, though that has been criticized<sup>10</sup>. More recently, observations have restricted surviving companions to be small, main-sequence stars<sup>11,12,13</sup>, ruling out giant companions, though still allowing the single-degenerate channel. Here we report the result of a search for surviving companions to the progenitor of SN 1006<sup>14</sup>. None of the stars within 4' of the apparent site of the explosion is associated with the supernova remnant, so we can firmly exclude all giant and subgiant companions to the progenitor. Combined with the previous results, less than 20 per cent of type Ia events occur through the single degenerate channel.

Together with SN 1572 (Tycho Brahe's supernova), SN 1604 (Kepler's supernova) and the recently identified SN 185, SN 1006 is one of only four known historical Galactic type Ia supernova events (SNeIa). It is also the only one whose Ia type has never been

disputed. While a survey of the stars close to the centre of Tycho’s supernova remnant (SNR) produced a likely candidate for the SN companion<sup>8,9</sup> and thus may be attributed to the single-degenerate channel, the absence of any ex-companion in the supernova remnant SNR 0509–67.5, in the Large Magellanic Cloud (LMC), down to very faint magnitudes, strongly suggests that the SN explosion there was produced by a double-degenerate system<sup>15</sup>. Although the aforementioned *direct* searches have excluded, up to now, red-giant companions, there is some evidence from nearby spiral galaxies that a fraction of SNeIa may have had companions of this type<sup>16</sup>. This hypothesis, however, is challenged by the absence of ultraviolet emission that would be expected at the beginning of the SN outburst<sup>17</sup>.

The distance to the remnant of SN 1006 ( $2.18 \pm 0.08$  kpc away, as determined from the expansion velocity and the proper motion of the ejecta<sup>18</sup>), is much more precisely known than that of SN 1572 SNR ( $2.83 \pm 0.70$  kpc). The interstellar extinction is also much smaller, which makes the distances to the stars less uncertain. To be a possible candidate, a star must first be at the correct distance and, depending on its spectral type and luminosity class, show some spectral peculiarity, or an enhancement of the abundances of Fe-peak elements such as that seen in star G of Tycho<sup>9</sup>. Because of its relative vicinity compared with SN 1572 and the lower extinction ( $A_v = 0.3$  mag, *vs.* 2.0–2.4 mag in Tycho), going down to a red magnitude  $m_R = 15$  allows us to include, up to the SN distance and beyond, all red giants, all subgiants, and also main-sequence stars down to an absolute magnitude  $M_R \simeq +3.1$ . Inspecting the 2MASS<sup>19</sup> photometric catalogue for

possible unevolved companions (Supplementary Information), we found no main-sequence stars brighter than  $m_R \simeq 16.4$ , which brings the limit down to  $M_R \simeq +4.5$ , corresponding to  $M_V \simeq +4.9$  (approximately equal to, or slightly less than, solar luminosity). Slightly evolved companions could be somewhat brighter:  $m_R \simeq 16.0$  (just about twice as luminous as the Sun). Only in the case of SNR 0509–67.5 in the LMC<sup>15</sup> has a fainter limit been reached in a direct search.

We derive the stellar atmosphere parameters of the sample stars (Fig. 1) using the high-resolution UVES spectroscopic data (Table 1). The spectra of four giants, and F- and G-type dwarfs of the sample are shown in Fig. 2, and in Supplementary Fig. S2, respectively. In Table 1 we also provide the radial velocities of sample stars measured from the UVES spectra, and distances determined from five photometric magnitudes, taking into account the stellar parameters (Supplementary Information). In Fig. 3 we compare the abundances of Fe-peak elements in the stars of our sample with the Galactic trends<sup>26</sup>, for F-, G- and K-type unevolved stars. Unlike in SN 1572, where star G shows an overabundance of Ni,  $[\text{Ni}/\text{Fe}] = 0.16 \pm 0.04$  (Here  $[\text{A}/\text{B}] = \log(N_A/N_B) - \log(N_A/N_B)_\odot$  for the number  $N$  of atoms of elements A and B, and subscript  $\odot$  indicates the solar value), the stars in SN 1006 are all within the dispersion of the  $[\text{Ni}/\text{Fe}]$  Galactic trend. No enhancement is seen for any other element. In Supplementary Fig. S3, we also show the Galactic trends of several  $\alpha$ -elements and we do not see any clear anomaly in these element abundances either.

None of the stars in the sample shows any significant rotation. High rotation

speeds have been claimed to be a characteristic of the surviving companions of SNeIa<sup>10</sup>, based on the assumptions that, owing to tidal interaction and in spite of the angular momentum loss due to mass transfer, the rotation periods before explosion are equal to the (short) orbital periods, and that the radius of the star remains basically unchanged after the explosion<sup>9</sup>. It has recently been shown<sup>27</sup>, however, that the impact of the SNIa ejecta on the companion does indeed reduce those speeds by a large factor, which would make the rotation criterion irrelevant.

Only four stars are at distances (marginally) compatible with that of the SNR. All of them are red giants: B16564 (G9-K0 III), B97341 (G9 III), B99810 (K1 III) and B93571 (K1 III) and none shows any spectroscopic peculiarity.

Two-dimensional hydrodynamic simulations of the impact of the ejecta of a SNIa on a red-giant binary companion have been performed<sup>28</sup>. More recently, the emission of supernova debris, arising from their impact with a similar companion, has been also considered<sup>17</sup>. As for the effects of the explosion on the companion star, the results agree: most of the envelope is stripped away and what is left are the degenerate core and a very small fraction (amounting to a few per cent) of the original envelope. This hydrogen-rich envelope initially extends up to  $\sim 350 R_{\odot}$  and then contracts on a thermal timescale. The star should be evolving at constant luminosity ( $\sim 10^3 L_{\odot}$ ) towards increasing effective temperatures for  $10^5$ – $10^6$  yr. The same conclusion is reached when extrapolating to the red-giant case the results of simulations of the impact of SNIa ejecta on a main-sequence companion<sup>29</sup>: the red giant should have been stripped off most of its hydrogen envelope.

Nothing similar to any of the above four normal red giants would be seen. On the other hand, the peculiar type of objects that would result from the interaction of the SNIa ejecta with a red-giant companion would be luminous enough to have been seen at the distance of SN 1006 and within our magnitude limit. A subgiant star similar to star G in Tycho would equally have been seen, but the only three subgiants in the sample (B20292, B15360 and B14707) lie much closer than the SNR. We are thus left only with main-sequence stars, which lie at shorter distances than the SNR, which have luminosities similar to, or lower than, the solar luminosity, and which are not predicted by any of the hydrodynamic simulations of the impact of SNIa ejecta with either a main-sequence star or a subgiant. In these hydrodynamic simulations<sup>28</sup>, a main-sequence companion of 1 solar mass is puffed up and heated, reaching  $\sim 5,000$  times the solar luminosity; it is then predicted to contract and cool down on a thermal time scale. It has been found<sup>30</sup> that the return to luminosities of the order of those prior to the explosion could be faster because of the short cooling times of the outermost layers of the star, but, even so, in only  $\sim 1000$  yr the object does not have enough time to become dimmer than the Sun (Supplementary Information).

Accordingly, SN 1006, the brightest event ever observed in our Galaxy, should have been produced either by mass accretion from an unevolved star, similar to, or less massive than, the Sun (with the above caveats), or by merging with another white dwarf. Adding this result to the evidence from the other direct searches, the single-degenerate channel appears either to encompass only a clear minority of cases (20% or less), or preferentially

it involves main-sequence companions with masses more probably below that of the Sun.

## References

- 1 Nomoto, K., Saio, H., Kato, M., & Hachisu, I. Thermal Stability of White Dwarfs Accreting Hydrogen-rich Matter and Progenitors of Type Ia Supernovae. *Astrophys. J.*, **663**, 1269–1276 (2007)
- 2 Patat, F., Chandra, P., Chevalier, R., et al. Detection of Circumstellar Material in a Normal Type Ia Supernova. *Science*, **317**, 924–926 (2007)
- 3 Branch, D., Livio, M., Yungelson, L.R., Boffi, F., Baron, E. In search of the progenitors of Type Ia supernovae. *Publ. Astron. Soc. Pacif.*, **107**, 1019–1029 (1995)
- 4 Pakmor, R., Kromer, M., Röpke, F. K., et al. Sub-luminous type Ia supernovae from the mergers of equal-mass white dwarfs with mass  $\approx 0.9M_{\text{solar}}$ . *Nature*, **463**, 61–64 (2010)
- 5 Ruiz-Lapuente, P. The quest for a supernova companion. *Science*, **276**, 1813–1814 (1997)
- 6 Greggio, L. The rates of Type Ia supernovae – II. Diversity of events at low and high redshifts. *Month. Not. Royal Astron. Soc.*, **406**, 22–42 (2010)
- 7 Brandt, T.D., et al. The ages of type Ia supernova progenitors. *Astrophys. J.*, **140**, 804–816 (2010)

- 8 Ruiz-Lapuente, P. *et al.* The binary progenitor of Tycho Brahe's 1572 supernova. *Nature*, **431**, 1069–1072 (2004)
- 9 González Hernández, J.I., *et al.* The chemical abundances of Tycho G in supernova remnant 1572. *Astrophys. J.*, **691**, 1–15 (2009)
- 10 Kerzendorf, W. *et al.* Subaru high resolution spectroscopy of star G in the Tycho supernova remnant. *Astrophys. J.*, **701**, 1665–1672 (2009)
- 11 Nugent, P.E., *et al.* Supernova SN 2011fe from an exploding carbon–oxygen white dwarf star. *Nature*, **480**, 344–347 (2011)
- 12 Li, W., *et al.* Exclusion of a luminous red giant as a companion star to the progenitor of supernova SN 2011fe. *Nature*, **480**, 348–350 (2011)
- 13 Edwards, Z.I., Pagnotta, A., Schaefer, B.E. The progenitor of the type Ia supernova that created SNR 0519–69.0 in the Large Magellanic Cloud. *Astrophys. J.*, **747**, L19–L23 (2012)
- 14 Stephenson, F.R. SN 1006: the brightest supernova. *Astron. Geophys.*, **51**, 5.27–5.32 (2010)
- 15 Schaefer, B.E., Pagnotta, A. An absence of ex-companion stars in the type Ia supernova remnant SNR 0509–67.5. *Nature*, **481**, 164–166 (2012)
- 16 Sternberg, A., *et al.* Circumstellar material in type Ia supernovae via sodium absorption features. *Science*, **333**, 856–859 (2011)

- 17 Kasen, D. Seeing the collision of a supernova with its companion star. *Astrophys. J.*, **708**, 1025–1031 (2010)
- 18 Winkler, P.F., Gupta, G., Long, K.S. The SN 1006 remnant: optical proper motions, deep imaging, distance, and brightness at maximum. *Astrophys. J.*, **585**, 324–335 (2003)
- 19 Cutri, R. M., Skrutskie, M. F., van Dyk, S., et al. 2MASS All-Sky Catalog of Point Sources. *VizieR Online Data Catalog*, **2246**, 0 (2003)
- 20 Allen, G.E., Petre, R., Gotthelf, E.V. X-ray synchrotron emission from 10–100 TeV cosmic ray electrons in the supernova remnant SN 1006. *Astrophys. J.*, bf 558, 739–752 (2001)
- 21 Monet, D.G. The 526,289,881 objects in the USNO–A2.0 Catalogue. *Bull. Amer. Astron. Soc.*, **30**, 1427 (1998)
- 22 Winkler, P.F., Long, K.S., Hamilton, A.J.S., Fesen, R.A. Probing multiple sight lines through the SN 1006 remnant by ultraviolet absorption spectroscopy. *Astrophys. J.*, **624**, 189–197 (2005)
- 23 Tabernero, H. M., Montes, D., González Hernández, J. I. Chemically tagging the Hyades Supercluster. A homogeneous sample of F6-K4 kinematically-selected northern stars. *Astron. Astrophys.*, in press (2012). Preprint at (<http://arxiv.org/abs/astro-ph/1245.4879>)
- 24 Sneden, C. PhD thesis. Univ. Texas, Austin (1973)

- 25 Kurucz, R.L. ATLAS89 Stellar Atmospheres Programs and 2 km s<sup>-1</sup> Grid. (CD-ROM, Smithsonian Astrophysical Observatory, Cambridge) (1993)
- 26 Neves, V., Santos, N.C., Sousa, S.G., Correia, A.C.M, Israelian, G. Chemical abundances of 451 stars from the HARPS GTO planet search program. Thin disk, thick disk, and planets *Astron. Astrophys.*, **497**, 563–81 (2009)
- 27 Pan, K.-C., Ricker, P., Taam, R. Impact of type Ia supernova ejecta on the binary companions in the single-degenerate scenario. *Astrophys. J.*, **750**, 151 (2012)
- 28 Marietta, E., Burrows, A., Fryxell, B. Type Ia supernova explosions in binary systems: the impact on the secondary star and its consequences. *Astroph. J. Suppl.*, **128**, 615–650 (2000)
- 29 Pakmor, R., Röpke, F.K., Weiss, A., Hillebrandt, W. The impact of Type Ia supernovae on main sequence binary companions. *Astron. Astrophys.*, **489**, 943–951 (2008)
- 30 Podsiadlowski, P. On the evolution and appearance of a surviving companion after a Type Ia supernova explosion. Preprint at (<http://arxiv.org/abs/astro-ph/0303660>) (2003)

**Supplementary Information** is linked to the online version of the paper at [www.nature.com/nature](http://www.nature.com/nature).

**Acknowledgements** This work was supported by the Spanish Ministerio de Ciencia e Innovación (MICINN), the Universidad Complutense de Madrid (UCM), and the Comunidad de Madrid. This work is based on observations collected with the UVES spectrograph at the VLT/UT2 8.2-m Kueyen Telescope (ESO run ID. 69.D-0397(A)) at the Paranal Observatory, Chile. We are grateful to the Cerro Paranal Observatory staff and to the User Support Department of ESO for their help.

**Author Contributions** J.I.G.H. performed the chemical abundance analysis of the observed UVES spectra and determined the distances to the targets. J.I.G.H. and P.R.L. wrote the paper. P.R.L. was the Principal Investigator of the ESO proposal. R.C. and J.M. also participated in the ESO proposal. H.M.T. and D.M. derived the stellar parameters and created figures with the observed spectra. R.C. and P.R.L. contributed to the astrophysical interpretation of the results. J.M. and L.R.B. collected the photometric data and created figures with the field and the supernova remnant. All the authors provided helpful comments and contributed to improve the text of the final version paper.

**Author information** Correspondence and requests should be addressed to J.I.G.H and P.R.L (jonay@iac.es; pilar@am.ub.es)

**Table 1 | Parameters of the sample stars.**

Name	$T_{\text{eff}}$	$\log g$	$v_{\text{turb}}$	[Fe/H]	$v_{\text{rad}}$	$d$
	[K]	[cgs]	[km/s]	[dex]	[km/s]	[kpc]
B09472	5853±75	4.52±0.17	1.211±0.105	-0.04±0.06	-20.74±2.14	1.23±0.53
B11408	4677±68	2.91±0.23	2.136±0.082	-0.29±0.05	-123.54±1.48	1.62±0.68
B05723	5910±87	4.50±0.23	1.249±0.107	0.30±0.07	-12.81±3.06	0.76±0.32
B17720	5300±86	4.65±0.22	1.190±0.193	0.33±0.06	-60.13±1.30	0.58±0.25
B16564	4845±39	3.13±0.16	1.607±0.049	-0.37±0.03	-116.07±1.86	3.03±1.27
B97338	5707±42	4.21±0.12	1.292±0.054	0.01±0.04	-5.53±2.25	1.05±0.45
B05518	6327±63	4.85±0.13	1.386±0.090	0.14±0.04	-4.38±1.92	0.50±0.21
B20292	5196±33	3.67±0.09	1.372±0.051	-0.66±0.03	2.92±2.52	1.13±0.48
B14130	6177±44	4.61±0.09	1.528±0.052	0.31±0.03	-21.26±2.09	0.89±0.38
B03395	5517±49	4.36±0.13	1.165±0.074	0.22±0.04	-56.18±5.21	0.95±0.41
B97341	4881±51	2.98±0.18	1.641±0.057	-0.16±0.04	-41.76±1.96	2.48±1.04
B99810	4658±39	2.51±0.15	1.782±0.039	-0.72±0.03	33.53±1.50	2.42±1.02
B15360	4960±70	3.40±0.21	1.886±0.086	0.07±0.05	-37.03±1.61	1.29±0.54
B93571	4579±58	2.51±0.22	2.182±0.066	-0.21±0.05	-100.33±1.58	2.39±1.01
B18024	6083±58	4.44±0.13	1.545±0.095	-0.36±0.04	22.61±2.35	0.60±0.26
B08277	5693±34	4.39±0.09	1.123±0.044	0.17±0.03	-49.50±2.08	0.45±0.19
B24215	5729±45	4.44±0.12	1.189±0.058	0.16±0.04	3.02±2.39	0.95±0.41
B14707	5065±47	3.36±0.15	1.270±0.060	0.16±0.04	22.14±1.83	1.37±0.58
B90474	5051±38	3.05±0.12	1.874±0.046	-0.29±0.03	-98.10±1.95	4.78±2.00
B90102	5650±33	4.21±0.10	1.076±0.049	-0.11±0.03	85.57±1.16	0.91±0.39
B10074	5601±63	4.52±0.14	1.036±0.102	0.05±0.05	-30.26±1.38	0.71±0.30
B95979	6776±94	4.19±0.16	1.832±0.131	0.02±0.06	-32.94±6.81	0.94±0.40
B09749	6163±65	4.53±0.14	1.362±0.082	0.14±0.05	-13.15±2.60	0.40±0.17
B26090	6101±39	4.58±0.09	1.238±0.053	0.15±0.03	-48.08±2.52	0.37±0.16

**Table 1 | Parameters of the sample stars.** We provide the stellar atmosphere parameters (effective temperature,  $T_{\text{eff}}$ , surface gravity,  $\log g$ , and microturbulent velocity,  $v_{\text{turb}}$ ), metallicities, [Fe/H], radial velocities,  $v_{\text{rad}}$ , and distances,  $d$ , of the sample stars, together with 1- $\sigma$  uncertainties. The stellar parameters and metallicities were obtained from Fe I and Fe II excitation and ionization equilibria, using the STEPAR<sup>23</sup> code, which makes use of the MOOG<sup>24</sup> code and ATLAS9 model atmospheres<sup>25</sup>. Our analysis has been performed assuming local thermodynamic equilibrium (LTE). SN 1006 is located about 500 pc above the Galactic plane. Unlike the case of SN 1572, which lies close to the Galactic plane, the radial velocities of the stars along the line of sight do not follow a regular pattern (this can be seen in the sixth column), since most of them belong either to the thick disc or to the halo of the Galaxy (see the dispersion in metallicities in the fifth column). Two of the observed stars, B98824 and B21185, are spectroscopic binaries and were discarded as possible companion stars of the progenitor of SN 1006 (Supplementary information).

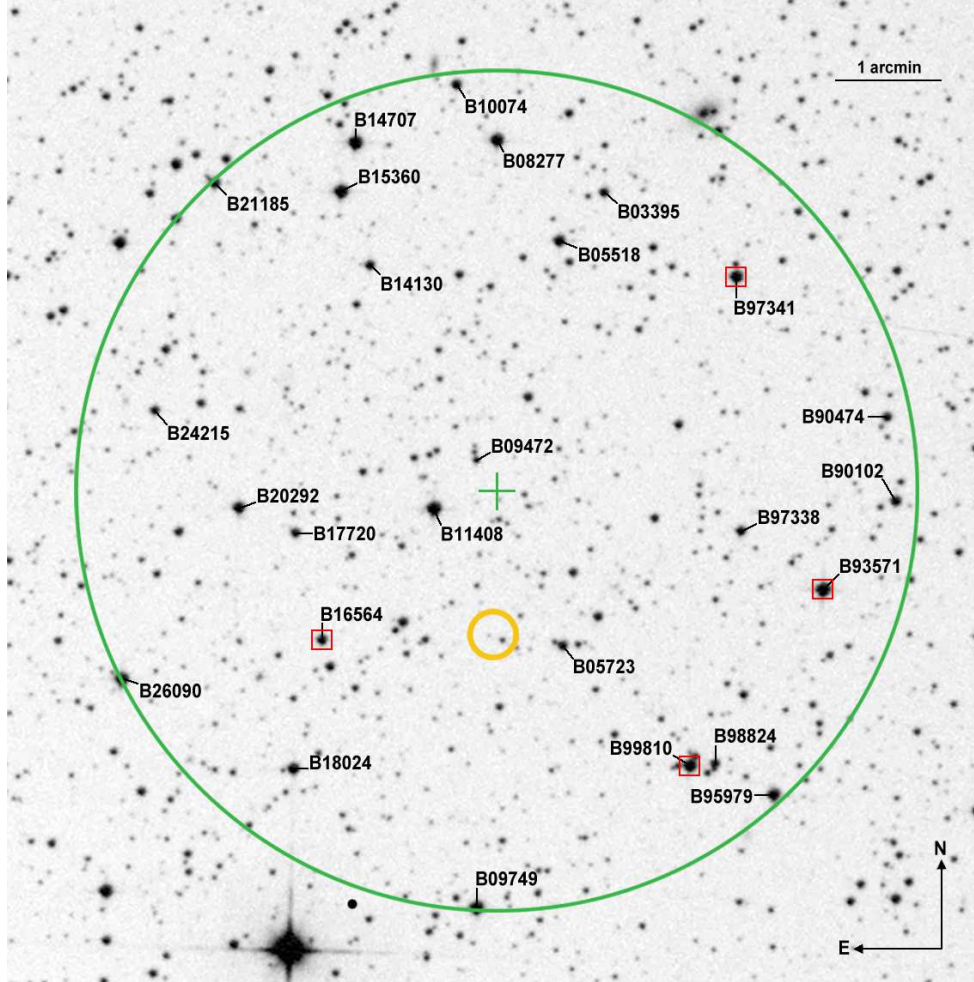


Figure 1: | **DSS2 R-band image of the SN 1006 field.** The positions and names of the 26 stars included in the spectroscopic survey (selected from the USNO-A2.0 Catalogue<sup>21</sup>) are given. The centre of our search is the geometrical centre of the quite symmetrical X-ray emission of the SNR<sup>20</sup> (green cross), at RA = 15<sup>h</sup> 2<sup>m</sup> 55<sup>s</sup>, Dec = -41° 55' 12". Also shown are the boundary of the surveyed region (large green circle) and the geometrical centre of the H-alpha emission<sup>18</sup> (small yellow circle). Giant stars are marked by red squares. See also Supplementary Fig. S1, for a full view of the SNR. Another centre has been proposed more recently<sup>22</sup>, based on the distribution of the ejecta along the line of sight. It is, however, still located within our surveyed area. For a star at a distance  $d \simeq 2.2$  kpc and a velocity perpendicular to the line of sight of  $\sim 100$  km s<sup>-1</sup> (roughly the orbital velocity before the explosion), the angular displacement on the sky in 1000 years would be 10" only. However, given the asymmetry of the SNR, and also that in core-collapse SNe the distance between the compact object and the X-ray centroid of the SNR can be 15% of the radius of the SNR or more, we adopted a much wider radius for the search: 4'. That amounts to 27% of the radius of the SNR, which is 15' (Supplementary Fig. S1). Positions, magnitudes and angular distances to the centre of the survey are given in Supplementary Table S1.

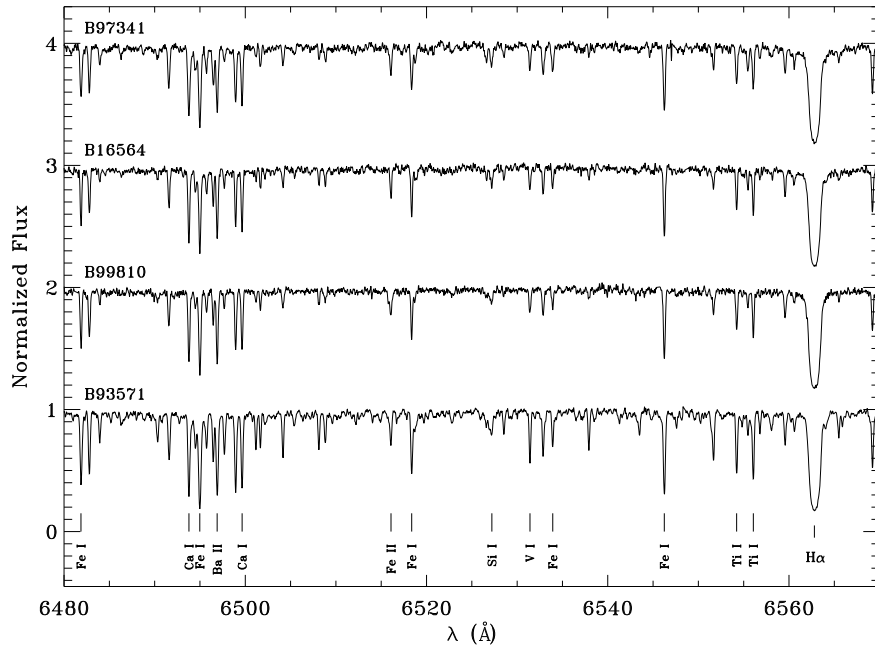


Figure 2: | **Observed UVES spectra of the candidate giant stars.** The spectra are labelled by their names in Table 1 and sorted in decreasing effective temperature order from top to bottom. These high-resolution spectra were obtained at the 8.2-m Kueyen VLT (UT2) telescope equipped with UVES at the Cerro Paranal Observatory in Chile. They were obtained on 13, 14, 25, 28–30 April 2002 and on 1 May 2002, covering the spectral regions 3295–5595 Å, 5680–6645 Å, 6705–8515 Å, and 8675–10420 Å at resolving power  $\lambda/\Delta\lambda \approx 43\,000$ . The S/N of the spectra is in the range 50–170 and typically 80. The data were reduced in a standard manner, and later normalized within IRAF, using low-order polynomial fits to the observed continuum.

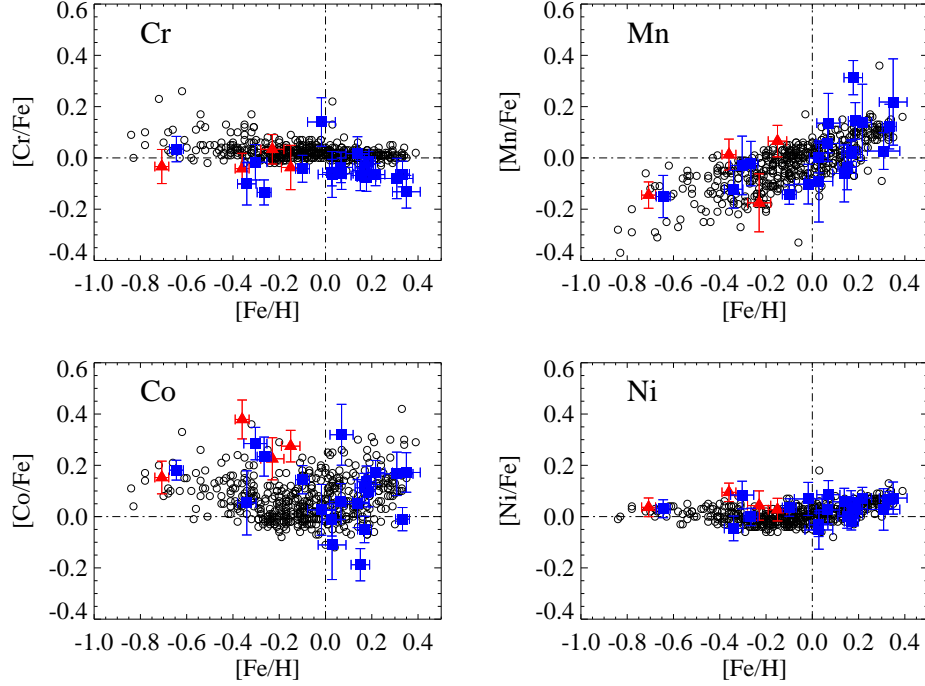


Figure 3: | **Stellar abundance ratios  $[X/Fe]$  of several Fe-peak elements.** The chemical abundances have been derived using the EW technique for all of the elements. We performed a differential analysis on a line-by-line basis, using the solar UVES spectrum of the Moon as reference (see the Supplementary Section 3 for more details). The abundances of several Fe-peak elements are listed in Supplementary Table S4b relative to iron are compared with the Galactic trends of these elements in the relevant range of metallicities<sup>26</sup>. Red triangles correspond to the four giant stars whose distances are marginally compatible with that of the remnant of SN 1006. Blue squares, to the rest of the stars in the sample. The error bars are the 1- $\sigma$  uncertainties associated with the dispersion of the measurements from different spectral features.

# SUPPLEMENTARY INFORMATION

## 1. Luminosities of the surviving companions

As stated in the main text, hydrodynamic simulations<sup>28</sup> of the interaction of the SNIa ejecta with either a main-sequence or a subgiant companion predict a significant injection of energy into the outer layers of the companion star that remain gravitationally bound after the impact. That results in a large excess in radius and in luminosity of the companion, as compared with the values corresponding to its mass and evolutionary stage, in hydrostatic and thermal equilibrium (the estimate is as high as  $\sim 5,000 L_{\odot}$ ). Simulations<sup>29</sup> of the collision of the material ejected by a SNIa with a main-sequence companion are entirely consistent with earlier ones<sup>28</sup>, the differences in the amount of mass stripped from the companion being due only to the more compact initial stellar models adopted for the simulations. The question still remains of how fast thermal equilibrium is restored (hydrostatic equilibrium is recovered very shortly after the collision with the SNIa ejecta). This issue has been explored for the case of main-sequence and subgiant companions<sup>30</sup>. Contrary to the assumption<sup>28</sup> that the governing time scale for the evolution in luminosity should be the thermal time scale of the whole stellar envelope, it is found that the luminosity can decrease much faster, due to the short cooling times of the outermost layers, so that in a much reduced time it could return (roughly) to its pre-explosion value.

The luminosity evolution depends on the amount of mass stripped, on the energy injected into the bound layers and on the cooling times of the outermost part of the stellar

envelope. For values matching the results of the hydrodynamic simulations<sup>28</sup> (and for a subgiant companion), the luminosities predicted<sup>30</sup> for a time  $\sim 1000$  yr after the SNIa explosion are within  $\sim 10\text{--}25L_{\odot}$ . Thus, even allowing for a wide margin of uncertainty, nothing below solar luminosity is to be expected.

A possibility has been suggested, within the SD channel, involving a low luminosity companion of the exploding white dwarf at the time of the SNIa<sup>31,32</sup>. The idea is that mass transfer from the companion spins up the accreting white dwarf, making the critical mass for explosive carbon ignition,  $M_{\text{crit}}$ , higher than the Chandrasekhar mass ( $M_{\text{Ch}} \simeq 1.4 M_{\odot}$ ). If mass transfer ceases when the mass of the white dwarf,  $M$ , is still lower than the  $M_{\text{crit}}$  corresponding to its spin rate (but higher than  $M_{\text{Ch}}$ ), there should be some time interval  $\tau$  between the end of mass accretion and the SNIa, required for spinning down until  $M_{\text{crit}} = M$ . It is then speculated<sup>32</sup> that  $\tau$  could be long enough for the companion (if it were a red giant or even a subgiant star) to have become a white dwarf. It must be noted that solid-body rotation only very slightly increases  $M_{\text{crit}}$  above  $M_{\text{Ch}}$  ( $M_{\text{crit}} = 1.47 M_{\odot}$ ). Only differential rotation can significantly increase  $M_{\text{crit}}$ <sup>33,34</sup>, but, in any case, the upper limit to the time scale for angular momentum redistribution and loss appears to be  $\sim 10^6$  yr only<sup>33</sup>. That would be enough, if the mass donor were a red-giant star and mass transfer stopped owing to contraction of the envelope when its mass becomes too low to sustain the red-giant structure<sup>31</sup>, to have a companion with a radius much smaller than the Roche lobe radius, but it would not be much less luminous than during the previous stage yet. To assume arbitrarily long time scales for angular

momentum redistribution and loss (thus allowing the companion star to become a white dwarf) is not supported by current models<sup>35,36</sup>.

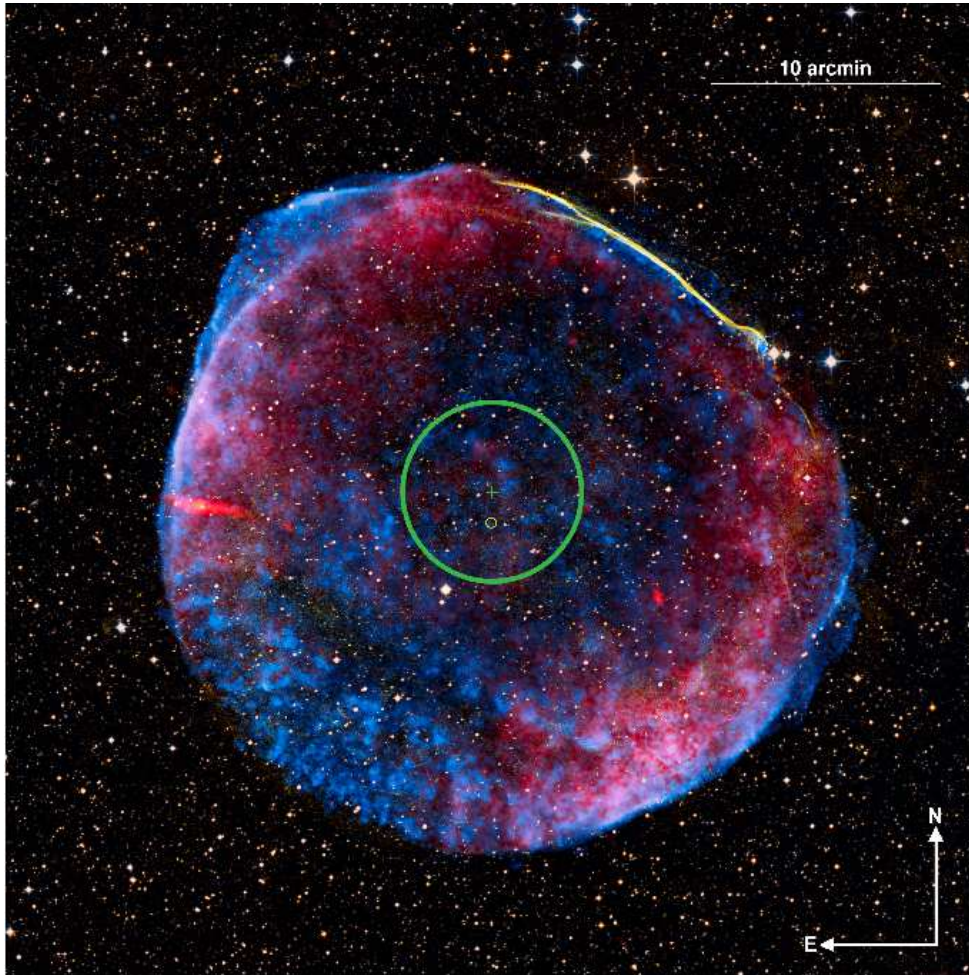


**Figure S1 | The remnant of the SN1006** The surveyed area is indicated by the large green circle. The centre of the survey (the centroid of the X-ray emission) is marked with a green cross, and that of the  $H\alpha$  emission, by the small yellow circle. This is a composite image of the SN 1006 supernova remnant, which is located about 7000 light years from Earth. Shown here are X-ray data from NASA's Chandra X-ray Observatory (blue), optical data from the University of Michigan's 0.9 metre Curtis Schmidt telescope at the NSF's Cerro Tololo Inter-American Observatory (CTIO; yellow) and the Digitized Sky Survey (orange and light blue), plus radio data from the NRAO's Very Large Array and Green Bank Telescope (VLA/GBT; red). Image credit: X-ray: NASA/CXC/Rutgers/G.Cassam-Chenaï, J.Hughes et al.; Radio: NRAO/AUI/NSF/GBT/VLA/Dyer, Maddalena & Cornwell; Optical: Middlebury College/F.Winkler, NOAO/AURA/NSF/CTIO Schmidt & DSS

## 2. Distance determinations of the sample stars

We have estimated the distances of the sample stars from the photometric magnitudes in five different filters: Johnson  $m_B$  and  $m_R$ , and  $m_J$ ,  $m_H$  and  $m_K$  from the 2MASS<sup>19</sup> catalogue (see Supplementary Table S2). The masses of the stars were estimated using a code<sup>37,38,39</sup> kindly provided by C. Allende-Prieto, according to their stellar parameters: effective temperature,  $T_{\text{eff}}$ , and surface gravity,  $\log g$ , and their metallicity,  $[\text{Fe}/\text{H}]$ , and assuming for all stars the uncertainties of 100 K, 0.3 dex and 0.1 dex in  $T_{\text{eff}}$ ,  $\log g$  and  $[\text{Fe}/\text{H}]$ , respectively. The calculations are based on solar-scaled theoretical isochrones<sup>40</sup>. The radii were then derived from the surface gravity and mass. This radius, together with the spectroscopic estimate of the effective temperature, provides the intrinsic bolometric luminosity in the ranges  $0.3 < L_{\star}/L_{\odot} < 1.4$  for dwarfs,  $4 < L_{\star}/L_{\odot} < 14$  for subgiants, and  $19 < L_{\star}/L_{\odot} < 69$  for giants.

In the Supplementary Table S3, we show the distance determinations for the different filters, using the bolometric corrections for models without overshooting<sup>41</sup>, for our preferred value of the colour excess,  $E(B - V) = 0.096$  mag, and other sets of the relevant parameters. We compute the magnitude corrected for extinction in each filter as  $m_{V,0} = m_V - A_V$ , where  $A_V = 3.12 E(B - V)$  is the extinction in the Johnson  $V$  filter. We adopt the following values for other filters<sup>42</sup>:  $A_B/A_V = 1.31$   $A_R/A_V = 0.84$ ,  $A_J/A_V = 0.32$ ,  $A_H/A_V = 0.27$  and  $A_K/A_V = 0.21$ . We adopt errors in  $m_B$  and  $m_R$  of 0.03. The error in the distance from each filter takes into account uncertainties of 100 K

and 0.3 dex in the stellar parameters, and uncertainties of  $0.2 M_{\odot}$  and 0.05 in mass and reddening, respectively, plus the individual errors of the photometric magnitudes. The final average distance of each star is given in Table 1, and Supplementary Tables S2 and S3 give the mean distances weighted by the individual uncertainties in different filters. We note that distance determinations from different filters are consistent and the final errors in the distances mostly reflect the systematic uncertainties.

The possibility that the proposed companion, Tycho G, of the SNIa SN 1572 had lost part of its envelope,  $\Delta M = -0.2 M_{\odot}$ , due to the impact of the supernova ejecta<sup>28,29,30</sup>, and that that would affect its derived distance, has been discussed<sup>9</sup>. It was concluded that the lower mass does not produce a significant change in the derived average distance, assuming that the subgiant companion star is able to almost completely recover thermal equilibrium between  $\sim 10^2$  and  $\sim 10^3$  yr after the white dwarf explosion<sup>30</sup>. We have done similar calculations and checked that this statement also applies to the sample stars in the SN 1006 field.

Finally, we inspected the 2MASS<sup>19</sup> catalogue to search for any possible main-sequence candidate to be the companion of SN 1006. For that, we extracted the 2MASS JHK magnitudes of the stars within the 4 arcmin radius around the centre of SN 1006 and computed the effective temperature from the IRFM<sup>43</sup> assuming that all stars in the field are solar-metallicity ( $[\text{Fe}/\text{H}] = 0$ ), main-sequence ( $\log g = 4.5$ ) stars. We determined their masses and luminosities as previously indicated and saw that there are only roughly 15 stars with magnitudes  $m_R$  in the range 16.3–17.5 ( $m_K$  in the range 15.1–15.7) and  $T_{\text{eff}}$

in the range 5250–6450 K. The same exercise has been repeated for slightly evolved stars, with  $\log g = 4$ . In this case, there are just 3 stars with magnitudes  $m_R$  in the range 16.0–16.3 ( $m_K$  in the range 14.8–15.1) and  $T_{\text{eff}}$  in the range 5350–5500 K. This upper-limit in the apparent magnitude corresponds to an absolute magnitude of  $M_R = +4.1$ . The case for  $\log g = 3.5$  produces stars at distances far beyond that of SN 1006. Therefore, as stated in the main text, any possible main-sequence companion at the distance of the SNR should be about as luminous as the Sun or less. Slightly evolved companions should have roughly twice the solar luminosity at most.

### 3. Determination of stellar parameters and element abundances of the sample stars

The stellar atmosphere parameters of the sample stars were obtained from the Fe I and Fe II excitation and ionization equilibria. We derive the equivalent widths (EWs) of the Fe I and Fe II lines with the ARES code<sup>44</sup> using a line list with 263 Fe I and 36 Fe II lines<sup>45</sup>. The parameters were computed using the STEPAR code<sup>23</sup>. This code employs the 2002 version of the MOOG code<sup>24</sup>, and a grid of Kurucz ATLAS9 plane-parallel model atmospheres<sup>25</sup>. Our analysis has been performed assuming local thermodynamic equilibrium (LTE). The parameters are shown in columns 2–4 of Table 1.

The chemical abundances have been derived by computing the EWs of spectral lines using the ARES code<sup>44</sup> for all the elements. Once the EWs are measured, we use the LTE MOOG code<sup>24</sup> to compute the chemical abundance provided by each spectral

line, using the appropriate ATLAS9 model atmosphere<sup>25</sup> for each star. We determine the mean abundance of each element relative to its solar abundance (using the UVES spectrum of the Moon) by computing the line-by-line mean difference. In Supplementary Tables S4a and S4b, we provide the average abundances of each element, together with the errors associated with the dispersion of the measurements from different spectral features. In Fig. 3 and Supplementary Fig. S3 we compare the abundance ratios  $[X/Fe]$  with the Galactic trends<sup>26</sup> and we do not see any clear signature of enhancement in the abundances of  $\alpha$ -elements or Fe-peak elements in any of the sample stars. The high scatter in the abundance ratios of some elements is related to the small available number of lines in the spectra.

### Supplementary References

- 31 Justham, S. Single degenerate type Ia supernovae without hydrogen contamination. *Astrophys. J. (Letters)*, **730**, L34–L38 (2011)
- 32 Di Stefano, R., Voss, R., Claeys, J.S.W. Spin-up/spin-down models for Type Ia supernovae. *Astrophys. J.*, **738**, L1–L4 (2011)
- 33 Yoon, S., Langer, N. Presupernova evolution of accreting white dwarfs with rotation. *Astron. Astrophys.*, **419**, 623–644 (2004)
- 34 Yoon, S., Langer, N. On the evolution of rapidly rotating massive white dwarfs towards supernovae or collapses. *Astron. Astrophys.*, **435**, 967–985 (2005)

- 35 Saio, H., Nomoto, K. Off-center carbon ignition in rapidly rotating, accreting carbon-oxygen white dwarfs. *Astrophys. J.*, **615**, 444–440 (2004)
- 36 Piro, A.L. The internal shear of Type Ia supernova progenitors during accretion and simmering. *Astrophys. J.*, **679**, 616–625 (2008)
- 37 Allende-Prieto, C., Asplund, M., Fabiani Bendicho, P. S4N: A spectroscopic survey of stars in the solar neighborhood. The Nearest 15 pc. *Astron. Astrophys.*, **423**, 1109–1117 (2004)
- 38 Reddy, B. E., Lambert, D. L., Allende Prieto, C. Elemental abundance survey of the Galactic thick disc. *Monthly Not. Royal Astron. Soc.*, **367**, 1329–1366 (2006)
- 39 Ramírez, I., Allende Prieto, C., Lambert, D. L. Oxygen abundances in nearby stars. Clues to the formation and evolution of the Galactic disk. *Astron. Astrophys.*, **465**, 271–289 (2007)
- 40 Bertelli, G., Bressan, A., Chiosi, C., Fagotto, F., Nasi, E. Theoretical isochrones from models with new radiative opacities. *Astron. Astrophys. Suppl.*, **106**, 275–302 (1994)
- 41 Bessell, M. S., Castelli, F., Plez, B. Model atmospheres broad-band colors, bolometric corrections and temperature calibrations for O - M stars. *Astron. Astrophys.*, **333**, 231–250 (1998)
- 42 Schaifers, K., *et al.* *Astronomy and Astrophysics*. C: Interstellar Matter, Galaxy,

- Universe, in Landolt–Börstein: Numerical Data and functional Relationships in Science and Technology. New Series (Springer–Verlag, Berlin) (1982)
- 43 González Hernández, J. I., & Bonifacio, P. A new implementation of the infrared flux method using the 2MASS catalogue. *Astron. Astrophys.*, **497**, 497–509 (2009)
- 44 Sousa, S.G., Santos, N.C., Israelian, G., Mayor, M., Monteiro, M.J.P.F.G. A new code for automatic determination of equivalent widths: Automatic Routine for line Equivalent widths in stellar Spectra (ARES). *Astron. Astrophys.*, **469**, 783–791 (2007)
- 45 Sousa, S.G. *et al.* Spectroscopic parameters for 451 stars in the HARPS GTO planet search program. Stellar [Fe/H] and the frequency of exo–Neptunes. *Astron. Astrophys.*, **487**, 373–381 (2008)
- 46 Gray, D. F. The observation and analysis of stellar photospheres. *Camb. Astrophys. Ser.*, **Vol. 20** (1992)

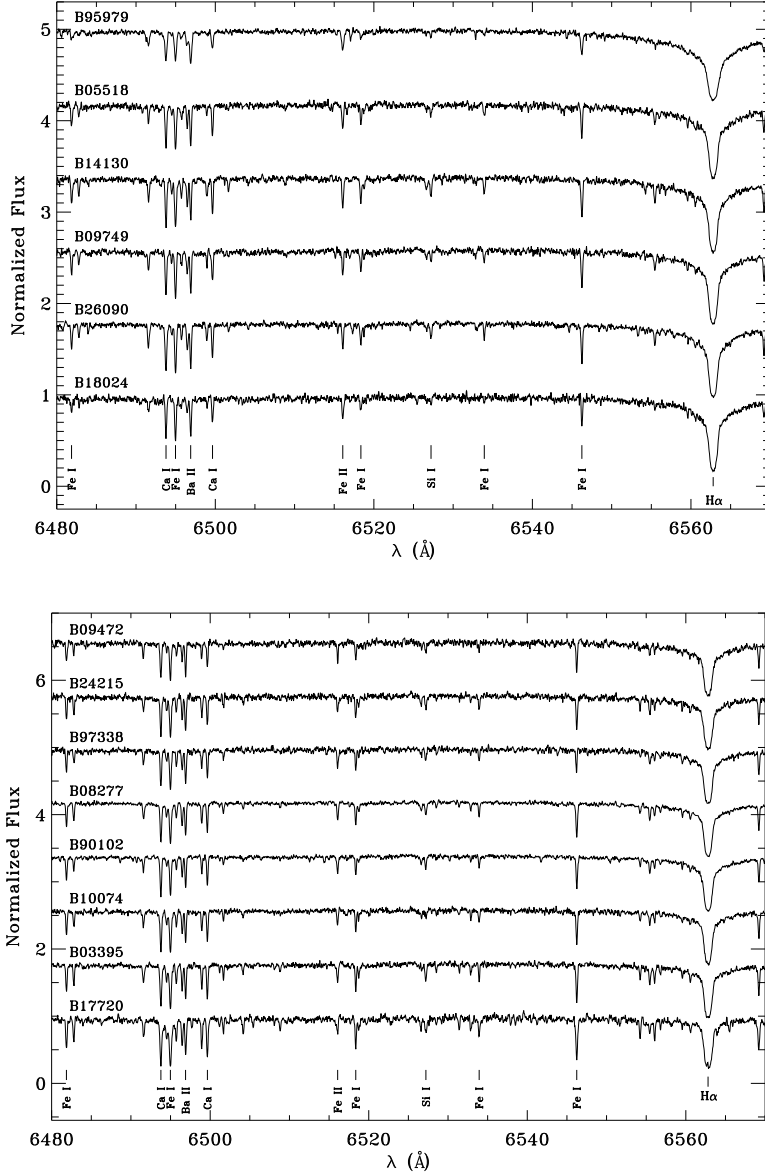


**Figure S2 | Observed UVES spectra of the candidate dwarf stars.** Spectra of the F-type (top panel) and G-type (bottom panel) sample stars, labelled by their names in Table 1, and sorted in decreasing effective temperature order from top to bottom. These high-resolution spectra were obtained at the 8.2-m Kueyen VLT (UT2) telescope equipped with UVES at the Cerro Paranal Observatory in Chile. They were obtained on 13, 14, 25, 28–30 April 2002 and on 1 May 2002, covering the spectral regions 3295–5595 Å, 5680–6645 Å, 6705–8515 Å, and 8675–10420 Å at resolving power  $\lambda/\Delta\lambda \approx 43\,000$ . The S/N of the spectra is in the range 50–170 and typically 80. The data were reduced in a standard manner, and later normalized within IRAF, using low-order polynomial fits to the observed continuum.

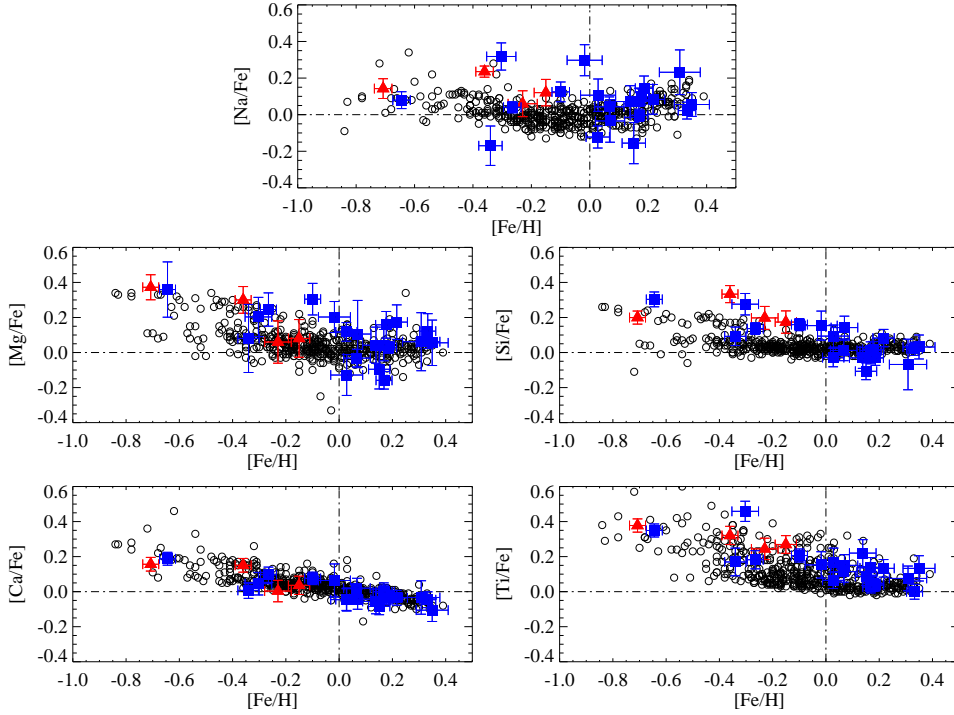


**Figure S3 | Stellar abundances of several elements.** These element abundances are listed in Supplementary Table S4a relative to iron and are compared with the Galactic trends of these elements in the relevant range of metallicities<sup>26</sup>. Red triangles correspond to the four giant stars whose distances are marginally compatible with that of the remnant of SN 1006. Blue squares, to the rest of stars in the sample.

**Table S1 | Astronomical positions, photometric magnitudes  $m_R$  and  $m_B$ , and angular distance to the center of the survey, of the sample stars**

Name	RA (J2000.0)	DEC (J2000.0)	$m_R^{**}$	$m_B^{**}$	$d_S$ [ $l$ ]
B09472	15:02:56.05	-41:54:52.5	14.9	16.2	0.38
B11408	15:02:58.25	-41:55:21.0	12.5	14.4	0.62
B05723	15:02:51.85	-41:56:39.6	13.7	15.3	1.57
B17720	15:03:05.35	-41:55:33.2	14.8	16.0	1.96
B16564	15:03:04.07	-41:56:34.7	14.3	15.6	2.18
B97338	15:02:42.59	-41:55:36.5	14.7	15.5	2.34
B05518	15:02:51.59	-41:52:49.3	13.8	14.8	2.46
B20292	15:03:08.22	-41:55:18.7	13.5	14.9	2.46
B14130	15:03:01.31	-41:53:01.3	14.5	15.6	2.47
B03395	15:02:49.27	-41:52:21.9	14.8	16.2	3.03
B97341	15:02:42.59	-41:53:11.0	12.9	14.9	3.07
B99810	15:02:45.34	-41:57:48.3	12.3	13.4	3.16
B15360	15:03:02.70	-41:52:19.3	12.6	14.6	3.21
B93571	15:02:38.42	-41:56:10.7	12.4	14.1	3.23
B18024	15:03:05.69	-41:57:48.0	13.7	14.1	3.27
B98824*	15:2:44.23	-41:57:50.7	13.3	14.6	3.32
B08277	15:02:54.72	-41:51:51.5	12.9	14.4	3.34
B24215	15:03:12.42	-41:54:22.1	14.7	16.0	3.38
B14707	15:03:01.92	-41:51:51.5	12.7	14.3	3.58
B90474	15:02:35.04	-41:54:33.1	14.8	16.0	3.77
B90102	15:02:34.64	-41:55:20.6	14.3	15.3	3.79
B10074	15:02:56.75	-41:51:19.1	14.7	15.8	3.89
B95979	15:02:41.10	-41:58:07.8	12.9	13.6	3.91
B09749	15:02:56.39	-41:59:09.0	12.7	13.7	3.96
B21185*	15:03:09.20	-41:52:12.7	13.8	15.3	3.99
B26090	15:03:14.42	-41:56:55.2	12.5	13.2	4.00

\*Spectroscopic binary

\*\*0.03 mag uncertainties

**Table S2 | Johnson magnitudes  $m_R$ ,  $m_B$ , and 2MASS<sup>19</sup> magnitudes  $m_J$ ,  $m_H$ ,  $m_K$ , spectral types and luminosity classes<sup>46</sup>, and distances of the sample stars**

Name	$m_R^*$	$m_B^*$	$m_J$	$m_H$	$m_K$	St. Type**	$d$ [kpc]
B09472	14.9	16.2	14.93±0.05	14.69±0.07	14.55±0.09	G1 V	1.23±0.53
B11408	12.5	14.4	11.05±0.03	10.32±0.03	10.21±0.02	K0-1 III	1.62±0.68
B05723	13.7	15.3	13.63±0.04	13.26±0.05	13.19±0.05	G0-1 V	0.76±0.32
B17720	14.8	16.0	13.61±0.03	13.20±0.03	13.12±0.03	G9-K0 V	0.58±0.25
B16564	14.3	15.6	12.84±0.02	12.22±0.03	12.13±0.02	G9-K0 III	3.03±1.27
B97338	14.7	15.5	13.49±0.02	13.17±0.03	13.09±0.04	G4-5 V	1.05±0.45
B05518	13.8	14.8	13.08±0.03	12.79±0.03	12.72±0.03	F6 V	0.50±0.21
B20292	13.5	14.9	12.40±0.02	11.89±0.02	11.83±0.02	G8 IV	1.13±0.48
B14130	14.5	15.6	13.81±0.03	13.49±0.03	13.51±0.04	F7 V	0.89±0.38
B03395	14.8	16.2	13.76±0.03	13.40±0.03	13.37±0.03	G7 V	0.95±0.41
B97341	12.9	14.9	11.94±0.02	11.38±0.03	11.29±0.02	G9 III	2.48±1.04
B99810	12.3	13.4	11.59±0.02	10.92±0.03	10.82±0.03	K1 III	2.42±1.02
B15360	12.6	14.6	11.43±0.02	10.88±0.02	10.74±0.02	K1 IV	1.29±0.54
B93571	12.4	14.1	10.82±0.02	10.16±0.03	10.01±0.02	K1 III	2.39±1.01
B18024	13.7	14.1	12.88±0.02	12.56±0.03	12.50±0.03	F8-9 V	0.60±0.26
B08277	12.9	14.4	12.20±0.03	11.82±0.02	11.71±0.02	G5 V	0.45±0.19
B24215	14.7	16.0	13.91±0.03	13.51±0.03	13.44±0.04	G4 V	0.95±0.41
B14707	12.7	14.3	11.46±0.02	10.98±0.03	10.88±0.02	K0 IV	1.37±0.58
B90474	14.8	16.0	13.43±0.03	12.91±0.03	12.80±0.03	G6 III	4.78±2.00
B90102	14.3	15.3	13.30±0.02	12.98±0.03	12.86±0.03	G5 V	0.91±0.39
B10074	14.7	15.8	13.46±0.03	13.09±0.02	12.99±0.03	G6 V	0.71±0.30
B95979	12.9	13.6	12.65±0.02	12.52±0.03	12.47±0.03	F1-2 V	0.94±0.40
B09749	12.7	13.7	11.90±0.02	11.60±0.03	11.57±0.03	F7-8 V	0.40±0.17
B26090	12.5	13.2	12.18±0.03	11.89±0.03	11.86±0.03	F8 V	0.37±0.16

\*0.03 mag uncertainties

\*\*St. Type refers to spectral type and luminosity class

**Table S3 | Photometric distances from different photometric magnitudes and their averages. The error given for each individual distance determination of each photometric magnitude is the 1- $\sigma$  uncertainty (see text). The errors of the average values are the 1- $\sigma$  uncertainties associated with the dispersion of the mean from the distances of different magnitudes and the average systematic error, respectively.**

Name	$d_{m_B}$ [kpc]	$d_{m_R}$ [kpc]	$d_{m_J}$ [kpc]	$d_{m_H}$ [kpc]	$d_{m_K}$ [kpc]	$d_{av}$ [kpc]
B09472	$1.02 \pm 0.45$	$0.95 \pm 0.41$	$1.46 \pm 0.62$	$1.52 \pm 0.64$	$1.46 \pm 0.62$	$1.23 \pm 0.28 \pm 0.53$
B11408	$1.75 \pm 0.75$	$1.67 \pm 0.71$	$1.63 \pm 0.69$	$1.54 \pm 0.64$	$1.52 \pm 0.63$	$1.62 \pm 0.10 \pm 0.68$
B05723	$0.74 \pm 0.32$	$0.59 \pm 0.25$	$0.86 \pm 0.36$	$0.84 \pm 0.35$	$0.84 \pm 0.35$	$0.76 \pm 0.11 \pm 0.32$
B17720	$0.55 \pm 0.24$	$0.60 \pm 0.26$	$0.58 \pm 0.25$	$0.59 \pm 0.25$	$0.58 \pm 0.25$	$0.58 \pm 0.02 \pm 0.25$
B16564	$2.78 \pm 1.19$	$3.31 \pm 1.40$	$3.11 \pm 1.30$	$3.00 \pm 1.24$	$2.98 \pm 1.23$	$3.03 \pm 0.19 \pm 1.27$
B97338	$0.97 \pm 0.42$	$1.17 \pm 0.50$	$1.04 \pm 0.44$	$1.05 \pm 0.44$	$1.04 \pm 0.44$	$1.05 \pm 0.07 \pm 0.45$
B05518	$0.51 \pm 0.22$	$0.50 \pm 0.21$	$0.51 \pm 0.21$	$0.50 \pm 0.21$	$0.50 \pm 0.21$	$0.50 \pm 0.01 \pm 0.21$
B20292	$1.09 \pm 0.47$	$1.13 \pm 0.48$	$1.15 \pm 0.48$	$1.13 \pm 0.47$	$1.13 \pm 0.47$	$1.13 \pm 0.02 \pm 0.48$
B14130	$0.89 \pm 0.39$	$0.85 \pm 0.36$	$0.90 \pm 0.38$	$0.88 \pm 0.37$	$0.91 \pm 0.38$	$0.89 \pm 0.02 \pm 0.38$
B03395	$0.99 \pm 0.43$	$0.94 \pm 0.40$	$0.93 \pm 0.40$	$0.94 \pm 0.40$	$0.96 \pm 0.41$	$0.95 \pm 0.02 \pm 0.41$
B97341	$2.59 \pm 1.10$	$2.21 \pm 0.94$	$2.58 \pm 1.08$	$2.55 \pm 1.05$	$2.54 \pm 1.05$	$2.48 \pm 0.16 \pm 1.04$
B99810	$1.59 \pm 0.68$	$2.22 \pm 0.95$	$3.08 \pm 1.30$	$2.98 \pm 1.25$	$2.96 \pm 1.23$	$2.42 \pm 0.67 \pm 1.02$
B15360	$1.48 \pm 0.63$	$1.23 \pm 0.52$	$1.28 \pm 0.54$	$1.26 \pm 0.52$	$1.23 \pm 0.51$	$1.29 \pm 0.11 \pm 0.54$
B93571	$2.34 \pm 1.00$	$2.54 \pm 1.08$	$2.42 \pm 1.02$	$2.38 \pm 0.99$	$2.30 \pm 0.96$	$2.39 \pm 0.09 \pm 1.01$
B18024	$0.48 \pm 0.21$	$0.65 \pm 0.28$	$0.65 \pm 0.27$	$0.64 \pm 0.27$	$0.64 \pm 0.27$	$0.60 \pm 0.07 \pm 0.26$
B08277	$0.47 \pm 0.21$	$0.42 \pm 0.18$	$0.47 \pm 0.20$	$0.46 \pm 0.19$	$0.45 \pm 0.19$	$0.45 \pm 0.02 \pm 0.19$
B24215	$0.96 \pm 0.42$	$0.92 \pm 0.39$	$0.98 \pm 0.41$	$0.96 \pm 0.40$	$0.96 \pm 0.40$	$0.95 \pm 0.02 \pm 0.41$
B14707	$1.41 \pm 0.61$	$1.38 \pm 0.58$	$1.36 \pm 0.57$	$1.36 \pm 0.56$	$1.34 \pm 0.56$	$1.37 \pm 0.03 \pm 0.58$
B90474	$4.43 \pm 1.89$	$5.22 \pm 2.21$	$4.87 \pm 2.03$	$4.77 \pm 1.97$	$4.70 \pm 1.94$	$4.78 \pm 0.29 \pm 2.00$
B90102	$0.84 \pm 0.37$	$0.94 \pm 0.40$	$0.92 \pm 0.39$	$0.94 \pm 0.40$	$0.92 \pm 0.39$	$0.91 \pm 0.04 \pm 0.39$
B10074	$0.72 \pm 0.31$	$0.78 \pm 0.33$	$0.69 \pm 0.29$	$0.69 \pm 0.29$	$0.68 \pm 0.29$	$0.71 \pm 0.04 \pm 0.30$
B95979	$0.81 \pm 0.36$	$0.84 \pm 0.36$	$1.01 \pm 0.42$	$1.04 \pm 0.43$	$1.03 \pm 0.43$	$0.94 \pm 0.11 \pm 0.40$
B09749	$0.40 \pm 0.18$	$0.40 \pm 0.17$	$0.41 \pm 0.17$	$0.40 \pm 0.17$	$0.41 \pm 0.17$	$0.40 \pm 0.00 \pm 0.17$
B26090	$0.29 \pm 0.13$	$0.34 \pm 0.14$	$0.43 \pm 0.18$	$0.43 \pm 0.18$	$0.43 \pm 0.18$	$0.37 \pm 0.07 \pm 0.16$

**Table S4a | Abundance ratios  $[X/Fe]$  of the sample stars in the SN 1006 survey for Na and the  $\alpha$ -elements Mg, Si, Ca and Ti. The errors provide the  $1\text{-}\sigma$  uncertainties associated with the dispersion of the measurements from different spectral features.**

Name	[Na/Fe]	[Mg/Fe]	[Si/Fe]	[Ca/Fe]	[Ti/Fe]
B09472	$0.30 \pm 0.08$	$0.20 \pm 0.09$	$0.14 \pm 0.18$	$0.06 \pm 0.21$	$0.17 \pm 0.18$
B11408	$0.32 \pm 0.08$	$0.20 \pm 0.14$	$0.28 \pm 0.11$	$0.05 \pm 0.11$	$0.43 \pm 0.13$
B05723	$0.23 \pm 0.00$	$0.06 \pm 0.21$	$-0.07 \pm 0.28$	$-0.03 \pm 0.09$	$0.08 \pm 0.03$
B17720	$0.06 \pm 0.04$	$0.06 \pm 0.16$	$0.01 \pm 0.18$	$-0.11 \pm 0.07$	$0.11 \pm 0.17$
B16564	$0.24 \pm 0.01$	$0.30 \pm 0.10$	$0.34 \pm 0.12$	$0.15 \pm 0.08$	$0.31 \pm 0.17$
B97338	$-0.12 \pm 0.06$	$0.45 \pm 0.42$	$-0.03 \pm 0.11$	$-0.05 \pm 0.14$	$0.07 \pm 0.10$
B05518	$-0.16 \pm 0.15$	$-0.10 \pm 0.15$	$-0.11 \pm 0.08$	$-0.08 \pm 0.07$	$0.07 \pm 0.14$
B20292	$0.08 \pm 0.05$	$0.30 \pm 0.26$	$0.30 \pm 0.09$	$0.19 \pm 0.06$	$0.36 \pm 0.09$
B14130	$0.02 \pm 0.05$	$0.12 \pm 0.13$	$0.01 \pm 0.07$	$-0.05 \pm 0.10$	$0.02 \pm 0.13$
B03395	$0.08 \pm 0.00$	$0.17 \pm 0.13$	$0.07 \pm 0.06$	$-0.03 \pm 0.04$	$0.13 \pm 0.12$
B97341	$0.12 \pm 0.08$	$0.08 \pm 0.00$	$0.20 \pm 0.16$	$0.04 \pm 0.10$	$0.24 \pm 0.11$
B99810	$0.14 \pm 0.06$	$0.37 \pm 0.09$	$0.20 \pm 0.07$	$0.16 \pm 0.08$	$0.38 \pm 0.13$
B15360	$-0.03 \pm 0.15$	$0.20 \pm 0.40$	$0.17 \pm 0.16$	$-0.04 \pm 0.09$	$0.14 \pm 0.15$
B93571	$0.06 \pm 0.07$	$0.06 \pm 0.16$	$0.22 \pm 0.14$	$0.00 \pm 0.10$	$0.22 \pm 0.15$
B18024	$-0.17 \pm 0.00$	$0.08 \pm 0.27$	$0.08 \pm 0.11$	$0.01 \pm 0.06$	$0.20 \pm 0.26$
B08277	$0.14 \pm 0.08$	$0.03 \pm 0.02$	$-0.03 \pm 0.09$	$-0.03 \pm 0.07$	$0.04 \pm 0.06$
B24215	$0.07 \pm 0.08$	$0.04 \pm 0.11$	$0.01 \pm 0.08$	$-0.00 \pm 0.09$	$0.11 \pm 0.15$
B14707	$0.10 \pm 0.02$	$0.16 \pm 0.09$	$0.03 \pm 0.09$	$-0.03 \pm 0.03$	$0.09 \pm 0.14$
B90474	$0.04 \pm 0.01$	$0.25 \pm 0.13$	$0.18 \pm 0.09$	$0.10 \pm 0.09$	$0.16 \pm 0.19$
B90102	$0.12 \pm 0.06$	$0.30 \pm 0.12$	$0.16 \pm 0.05$	$0.08 \pm 0.05$	$0.21 \pm 0.08$
B10074	$0.04 \pm 0.03$	$-0.03 \pm 0.01$	$0.01 \pm 0.09$	$0.02 \pm 0.08$	$0.10 \pm 0.14$
B95979	$0.11 \pm 0.09$	$-0.24 \pm 0.00$	$0.09 \pm 0.06$	$-0.05 \pm 0.07$	$0.15 \pm 0.18$
B09749	$0.07 \pm 0.00$	$0.04 \pm 0.13$	$-0.05 \pm 0.11$	$-0.06 \pm 0.14$	$0.22 \pm 0.23$
B26090	$-0.00 \pm 0.02$	$-0.16 \pm 0.06$	$-0.03 \pm 0.07$	$-0.00 \pm 0.07$	$0.03 \pm 0.06$

**Table S4b | Abundance ratios [X/Fe] (cont.) of the sample stars in the SN 1006 survey for the iron-peak elements Cr, Mn, Co and Ni.**

Name	[Cr/Fe]	[Mn/Fe]	[Co/Fe]	[Ni/Fe]
B09472	$0.14 \pm 0.21$	$-0.10 \pm 0.10$	$0.03 \pm 0.21$	$0.07 \pm 0.12$
B11408	$-0.00 \pm 0.15$	$-0.03 \pm 0.21$	$0.28 \pm 0.10$	$0.08 \pm 0.11$
B05723	$-0.09 \pm 0.11$	$0.22 \pm 0.22$	$0.17 \pm 0.12$	$0.03 \pm 0.19$
B17720	$-0.11 \pm 0.09$	$0.22 \pm 0.31$	$0.17 \pm 0.12$	$0.07 \pm 0.10$
B16564	$-0.03 \pm 0.16$	$0.01 \pm 0.10$	$0.38 \pm 0.18$	$0.09 \pm 0.10$
B97338	$-0.08 \pm 0.12$	$0.00 \pm 0.09$	$-0.01 \pm 0.13$	$-0.03 \pm 0.12$
B05518	$-0.11 \pm 0.08$	$-0.04 \pm 0.16$	$-0.19 \pm 0.13$	$0.00 \pm 0.12$
B20292	$0.00 \pm 0.15$	$-0.15 \pm 0.15$	$0.18 \pm 0.06$	$0.03 \pm 0.10$
B14130	$-0.03 \pm 0.08$	$0.12 \pm 0.16$	$-0.01 \pm 0.09$	$0.06 \pm 0.07$
B03395	$-0.07 \pm 0.05$	$0.14 \pm 0.29$	$0.17 \pm 0.06$	$0.07 \pm 0.07$
B97341	$-0.04 \pm 0.23$	$0.07 \pm 0.09$	$0.27 \pm 0.12$	$0.03 \pm 0.10$
B99810	$-0.01 \pm 0.18$	$-0.15 \pm 0.08$	$0.15 \pm 0.14$	$0.04 \pm 0.12$
B15360	$-0.06 \pm 0.10$	$0.14 \pm 0.21$	$0.32 \pm 0.28$	$0.09 \pm 0.12$
B93571	$0.04 \pm 0.08$	$-0.18 \pm 0.20$	$0.23 \pm 0.17$	$0.04 \pm 0.15$
B18024	$-0.01 \pm 0.27$	$-0.12 \pm 0.12$	$0.05 \pm 0.29$	$-0.05 \pm 0.13$
B08277	$-0.02 \pm 0.07$	$0.14 \pm 0.13$	$0.10 \pm 0.13$	$0.03 \pm 0.06$
B24215	$-0.06 \pm 0.12$	$0.02 \pm 0.07$	$0.11 \pm 0.11$	$0.06 \pm 0.11$
B14707	$-0.09 \pm 0.12$	$0.31 \pm 0.11$	$0.14 \pm 0.12$	$0.01 \pm 0.13$
B90474	$-0.11 \pm 0.14$	$-0.02 \pm 0.16$	$0.23 \pm 0.19$	$-0.00 \pm 0.09$
B90102	$-0.04 \pm 0.14$	$-0.14 \pm 0.05$	$0.14 \pm 0.12$	$0.04 \pm 0.09$
B10074	$-0.04 \pm 0.09$	$0.06 \pm 0.08$	$0.06 \pm 0.11$	$0.03 \pm 0.11$
B95979	$-0.06 \pm 0.19$	$-0.09 \pm 0.25$	$-0.11 \pm 0.27$	$-0.05 \pm 0.23$
B09749	$0.05 \pm 0.16$	$-0.06 \pm 0.20$	$0.05 \pm 0.21$	$0.06 \pm 0.09$
B26090	$-0.05 \pm 0.10$	$0.03 \pm 0.05$	$-0.05 \pm 0.10$	$-0.02 \pm 0.07$